Journal of Electron Spectroscopy and Related Phenomena 204 (2015) 269–276

Contents lists available at ScienceDirect

Journal of Electron Spectroscopy and Related Phenomena

journal homepage: www.elsevier.com/locate/elspec

Ultrafast molecular dynamics illuminated with synchrotron radiation

John D. Bozek[a,*], Catalin Miron[a,b]

[a] Synchrotron SOLEIL, l'Orme des Merisiers, Saint-Aubin, BP 48, 91192 Gif-sur-Yvette Cedex, France
[b] Extreme Light Infrastructure – Nuclear Physics, "Horia Hulubei" National Institute for Physics and Nuclear Engineering, 30 Reactorului Street, RO-077125 Măgurele, Jud. Ilfov, Romania

ARTICLE INFO

Article history:
Available online 28 August 2015

PACS:
31.50.Df
33.20.Tp
33.80.−b
34.50.Gb

Keywords:
Ultrafast
Molecular dynamics
Core excitation
Synchrotron radiation
Electron spectroscopy
Electron-ion coincidence

ABSTRACT

Synchrotron radiation is a powerful tool for studying molecular dynamics in small molecules in spite of the absence of natural matching between the X-ray pulse duration and the time scale of nuclear motion. Promoting core level electrons to unoccupied molecular orbitals simultaneously initiates two ultrafast processes, nuclear dynamics on the potential energy surfaces of the highly excited neutral intermediate state of the molecule on the one hand and an ultrafast electronic decay of the intermediate excited state to a cationic final state, characterized by a core hole lifetime. The similar time scales of these processes enable core excited pump-probe-type experiments to be performed with long duration X-ray pulses from a synchrotron source. Recent results obtained at the PLIEADES beamline concerning ultrafast dissociation of core excited states and molecular potential energy curve mapping facilitated by changes in the geometry of the short-lived intermediate core excited state are reviewed. High brightness X-ray beams combined with state-of-the art electron and ion-electron coincidence spectrometers and highly sophisticated theoretical methods are required to conduct these experiments and to achieve a full understanding of the experimental results.

1. Introduction

Molecular dynamics occur on a wide range of timescales spanning attoseconds to many seconds or even longer depending upon the processes involved. Typically, however, when discussing molecular dynamics of isolated molecules in the context of light-matter interactions, it is the motion of nuclei within the molecule, which occurs on the femtosecond ultrafast time-scale that is of interest. A pump-probe experiment to probe these molecular dynamics therefore requires femtosecond pulse durations and equivalent relative timing to be useful in the study of such processes. In order to interact with site-selected species in molecules though core-level excitation and ionization X-rays are a powerful tool to probe molecular dynamics using the well-established techniques of photoelectron, photoion and various particle and photon coincidence techniques. Synchrotron radiation is a common source of X-ray radiation and modern 3rd generation high-brightness storage rings typically have pulse durations on the order of 10s of ps, however, with repetition rates in the MHz to 500 MHz range, both too long to follow this type of molecular dynamics and at too high a repetition rate for high powered pump lasers to be synchronized on a pulse-by-pulse basis. Recently developed X-ray free electron lasers provide both short wavelengths and short pulse-durations [1–3] and are suitable for pump-probe experiments [4,5], but access to these sources is limited and, as shown below, not always necessary to access molecular dynamics in some small molecules. In spite of the mismatch between the time scales of ultrafast dynamics and synchrotron radiation pulse durations, extensive use has been made of X-rays from synchrotrons to study molecular dynamic processes. Several extensive reviews of the phenomena involved and recent advances have been published recently [6–8] and only an outline of the mechanisms involved are given below.

Nature provides an inherent pump-probe mechanism in the form of core level excitation to empty molecular orbitals below the ionization continuum as illustrated in Fig. 1. Upon excitation of a core electron from the ground state of the molecule to a core excited state, consisting of a molecular orbital below the ionization potential, a competition between two temporal processes is launched. The energetic core-hole state is highly unstable and will decay with a lifetime typically on the order of a few femtoseconds. The excited electron, populating a molecular orbital that was previously not occupied, changes the nature of the bonding in the molecule. Depending on the nature of the unoccupied molecular

* Corresponding author. Tel.: +33 169359702.
E-mail addresses: john.bozek@synchrotron-soleil.fr (J.D. Bozek), catalin.miron@synchrotron-soleil.fr (C. Miron).

http://dx.doi.org/10.1016/j.elspec.2015.07.012
0368-2048/

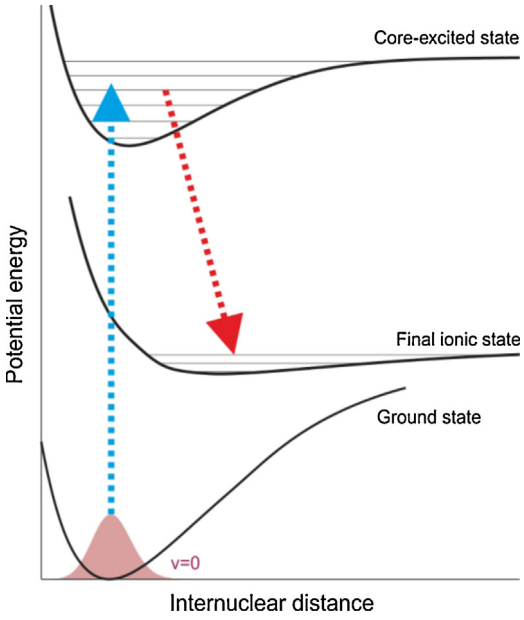

Fig. 1. Schematic representation of the potential energy curves for the initial ground state, intermediate core excited state and final cationic state with arrows indicating the excitation and deexcitation processes.

orbital a variety of dynamical process can be triggered. Unoccupied molecular orbitals can be antibonding orbitals and promotion of a core electron to this type of orbital initiates a dissociation of the molecule that begins immediately upon excitation of the electron. Empty molecular orbitals can also be bonding or non-bonding, inducing changes in the nuclear geometry, such as lengthening or shortening of the equilibrium bond length. Regardless of their bonding character, however, promotion of an electron from a core level to an empty molecular orbital launches nuclear dynamics in the molecule that occur on the ultrafast time scale of nuclear motion in molecules, femtoseconds.

The subsequent deexcitation of the core excited state to a more energetically favorable valence hole cationic state can be accomplished through Auger decay with ejection of an electron carrying away the excess energy of the transition. The Auger decay projects the electronic state of the molecule from the intermediate core excited state onto the potential energy surface of the final ionic state, which is often one of the manifold of lower ionic states (i.e. valence ionic states) of the molecule. The creation of holes in the valence shell of a molecule via the excitation of a core level electron to an empty molecular orbital is known as resonant photoemission and is a useful tool in studying ultrafast molecular dynamics.

As will be seen below, resonant photoemission provides exceptional detail about the nature of molecular potentials and dynamics when vibrational resolution of the final states is achieved. Observation of the vibration levels of the final cationic state provides a detailed probe of the nuclear dynamics by mapping the changes in the geometry upon excitation and deexcitation in the resonant photoemission process. State-of-the art synchrotron sources, X-ray beamlines and electron spectrometers are required to achieve the required resolution at the high photon energies used to excite core level electrons. The PLEIADES beamline [9] at synchrotron SOLEIL where much of the work reported here was done is one such facility. The beamline covers the energy range from 7 to 1000 eV providing linearly and circularly polarized light with high brightness and spectral resolution. End-stations for high-resolution electron spectroscopy and electron-ion coincidence spectroscopy designed for studying dilute gaseous samples were used for several of the studies reported here.

Interpretation of the experimental data to extract the underlying physical processes involved requires equally sophisticated theoretical methods. Recent developments in modeling core level excited states and their decay to cations final states involve high level ab initio computation of molecular potentials, time dependent nuclear dynamics and excitation and deexcitation probabilities. The intricacies of these exquisite theoretical methods are not discussed in the following discussion, but their results have been essential in interpreting the experiment spectra. Readers are directed to the original source materials referenced below for details on the theoretical methods.

A selection of examples have been chosen from recently reported studies from the PLEIADES beamline at Synchrotron SOLEIL to illustrate how high-resolution synchrotron radiation can be used both to study and capitalize on molecular dynamics in small molecules. Ultrafast dissociation, where core excitation initiates the fragmentation of a molecular bond is both discussed from a fundamental viewpoint and used as a tool to view new physics in these examples. High resolution resonant photoemission is demonstrated as a tool for investigation of the dynamics in core excited molecules and an illustration of how it can be used to study otherwise inaccessible valence ionization states of molecules is presented. Overall, in spite of the mismatch of the pulse duration of X-rays from synchrotron with nuclear dynamic processes in small isolated molecules these results illustrate that the use of state-of-the art experimental synchrotron X-ray sources and beamlines, electron and coincidence spectrometers and recently developed theoretical methods provides a means to study these processes in extraordinary detail.

2. Ultrafast dissociation

Ultrafast dissociation following excitation of a core electron to an antibonding molecular orbital was first identified in the molecule HBr in 1986 [10] following excitation of Br 3d electrons to the σ^* resonance at 70.6 eV. The molecule was chosen as an isoelectronic molecular analog of Kr where previous studies of Auger spectra of resonantly excited core level states had identified numerous new lines corresponding to Auger decays in which the excited electron participated in the decay or remained in an excited state as a spectator to the process [11]. Rather than observing the expected broad feature in the spectrum of HBr, however, a set of sharp lines were found and identified as resulting from Auger decay of atomic Br. The atomic lines were unambiguously identified when they were found to maintain a constant kinetic energy when the photon energy was changed as shown in Fig. 2.

A model of rapid dissociation of the molecule before the core hole lifetime limited Auger decay of the Br 3d core hole caused by the excitation of the Br 3d electrons onto the dissociative potential energy curves of the σ^* state has been suggested, as illustrated in Fig. 3. In this explanation of the surprising observation of atomic Br resonant Auger lines following core level excitation of HBr, excess energy from the projection of the electron distribution onto the dissociative curves is carried away as kinetic energy of the fragment atoms and the electron energies are determined solely by transitions between the atomic energy levels in the Br atom. Subsequent studies of the analogous CH_3Br molecule found similar atomic Auger lines but with reduced relative intensity compared to those found in HBr [12], attributed to the increased mass of the CH_3 moiety, versus H, separating from the Br atom, and hence reduced speed and lesser internuclear separation at the instant of Auger decay or the Br 3d core hole.

Ultrafast dissociation in HBr and its manifestations in electron spectroscopy continues to be an active area of research. A detailed study of electron emission from HBr in the vicinity of the σ^*

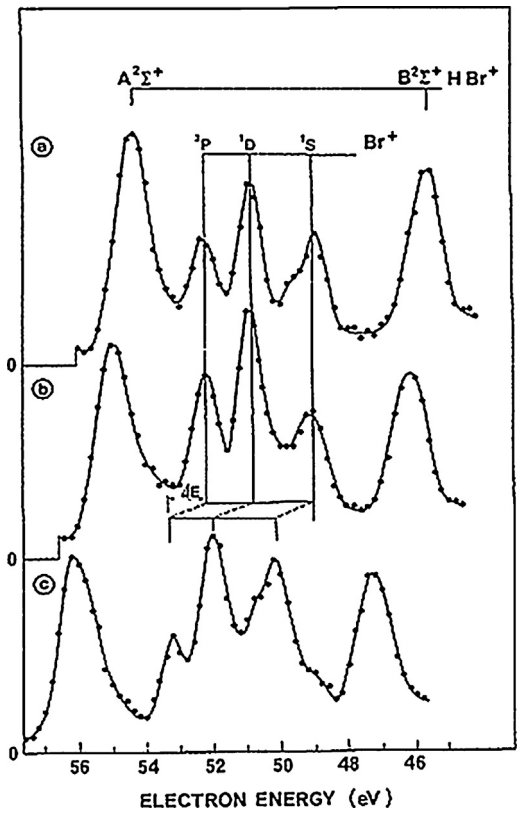

Fig. 2. Photoelectron spectra of HBr recorded at photon energies across the σ^* resonance, (a) 70 eV, (b) 70.6 eV and (c) 71.6 eV. The vertical lines show the positions of the atomic Auger lines from core excited atomic Br.
From Ref. [7].

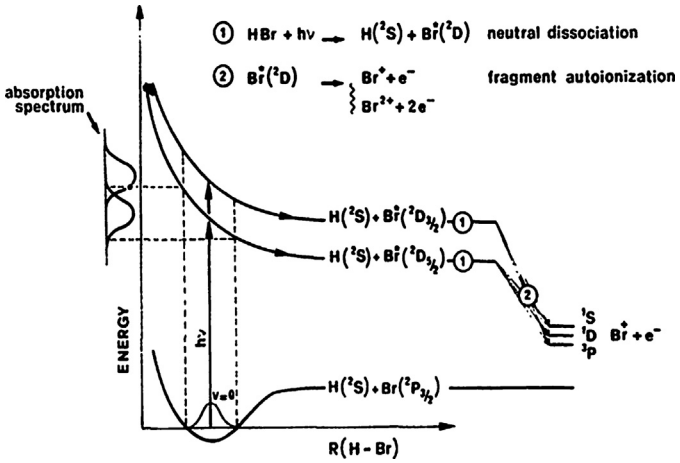

Fig. 3. Potential energy curves describing the processes observed in the ultrafast dissociation of HBr. Absorption of a photon, hν, projects the ground state wavefunction onto the dissociative upper curves that electronically decay to the atomic cationic states of Br indicated on the right.
From Ref. [7].

resonance including a two dimensional map of electron kinetic energy as a function of the exciting photon energy and angularly resolved electron spectra of the atomic lines has been reported recently [13]. A total of 16 atomic lines were identified in the 2D maps and the details of the electronic configurations of the final states assigned for most of them. Changes in the dissociation rate of the molecule as a function of photon energy across the broad σ^* resonance and its effect on the shape of the atomic lines was identified and attributed to the shapes of the repulsive potential energy curves of the intermediate excited state, different portions of which are probed with different photon energy. A very recent analysis of the lineshapes of isolated atomic Br lines in high-resolution electron spectra of HBr photoexcited to the $3d_{5/2} \rightarrow \sigma^*$ resonance at 70.50 eV photon energy found a lifetime broadening of 91 ± 5 meV for Br^* atoms in the $(3d_{5/2})^{-1}4s^24p^6$ configuration [14]. Detailed analysis of the sharp molecular lines present in the same spectrum allowed the instrument Gaussian contributions to the lineshape to be accurately determined resulting in an accurate determination of the Lorentzian component of the Voigt profile used to fit the atomic line and therefore a precise lifetime determination.

An extensive review of ultrafast dissociation following excitation of core level electrons into antibonding orbitals has been reported recently [7] outlining the discovery of the process in HBr and the subsequent extension of the method to other more complex molecules, clusters and molecules condensed on surfaces together with descriptions of concurrent theoretical advancements. Certain unique aspects of the phenomenon bear further discussion here, however.

One fascinating case of electronic decay of an atomic fragment after ultrafast decay following excitation of an O 1s electron to the antibonding $3\sigma_u$ (σ^*) state below the ionization threshold is found in for O_2. Electron emission from this core excited intermediate state exhibits the expected lines from both molecular and atomic final states with about 10% of the signal arising from electronic decay of atomic O^* [15]. The angular distribution of electron emission from the atomic fragments was examined and found to hold a surprising result. Excitation of an O 1s electron, or more correctly an electron for a $1\sigma_g$ delocalized orbital formed by the coherent superposition of the two atomic orbitals, to the $3\sigma_u$ state results in an ensemble of oriented excited molecules being created. The $1\sigma_g \rightarrow 3\sigma_u$ transition moment is proportional to $\cos^2\theta$ where θ is the angle between the polarization vector of the radiation and molecular axis of diatomic O_2, hence for linearly polarized light, molecules aligned with the polarization vector will be selectively excited. In core level excited O_2 the ultrafast dissociation and Auger decay occur on a much faster time scale than molecular rotation and hence the orientation of the molecule is preserved throughout these ultrafast steps. Atoms recoiling from the ultrafast dissociation process in the homonuclear O_2 molecule counter propagate along the bond axis which was aligned to the polarization of the X-ray beam by the core excitation. Auger decays of the excited atomic fragments will therefore occur in atoms moving along this orientation. Björnholm et al. were the first to observe a Doppler shift in the kinetic energies of Auger electrons from the atomic O^* fragments induced by the motion of the atoms toward or away from the electron detector when the detector was oriented in the plane of the polarization of the synchrotron radiation. Only a single broad peak was measured with the detector oriented perpendicularly to the polarization of the X-ray beam. A Doppler splitting of 0.75 eV was measured and used to estimate a kinetic energy of 8 eV for the O atoms corresponding to a speed of 0.14 Å/fs. Doppler shifts of Auger electron lines due to fast dissociation of core-excited states has since been observed in several other molecules including O_3, HF, CF_4, SF_6 [6] and CH_3Cl [16]. Doppler shifts of kinetic energies of photoelectrons from atoms and molecules dues to translational [17] and rotational recoil effects [18] have also been observed recently, but are not considered further here since they are not directly related to these molecular dynamics studies.

Ultrafast dissociation studies of core excited molecules have typically involved fragmentation along a single bond with the two fragments of the molecule partitioning the excess energy from the dissociative state between them as they separate along the axis of the bond with equal and opposite momenta. As the masses of the

fragments increase their velocities decrease for the same potential energy curves and hence the internuclear separation in the lifetime of the core hole state decreases resulting in a reduction in the fraction of fragment contribution to the recorded Auger electron signal. Recently reported measurements of ultrafast dissociation in dichloroethene [19] and 1-bromo-2-chloroethane [20] at the shallow halogen atom core levels, Cl 2p and Br 3d, have illustrated the need to consider additional mechanisms for the ultrafast ejection of excited atoms from these large polyatomic molecules. Coincident Auger electron – ion measurements in 1-bromo-2-chloroethane clearly confirmed the appearance of atomic lines from the excited Cl* atom when measured in coincidence with Cl^+ ions providing an unequivocal indication of ultrafast dissociation in this molecule. Theoretical modeling of the ground and excited state geometries and potential energy surfaces reproduced the neutral dissociation of the molecule upon core excitation of the Cl or Br core level electrons and found that in the early stages of dissociation the two halogen atoms remained almost stationary in the molecule while the carbon atoms moved around them. Further molecular dynamics calculations found that in 1-bromo-2-cholorethane the C-Cl* and C-Br* bonds are elongated at about the same rate as in CH_3Cl^* and CH_3Br^* respectively. The early stage motion of the carbon atoms was described as a rotation around the unexcited halogen atom allowing the carbon halogen bond around the excited atom to elongate and eventually fragment by the time Auger decay occurred on the excited atom. Molecular dynamics more complex than the simple axial recoil along the bond to the excited atom was therefore found to contribute to ultrafast dissociation in 1-bromo-2-chloroethane. This observation illustrates that ultrafast dissociation will not be limited simply to the study of ultrafast dynamics in hydrogen halides but will be applicable in ever more complex molecular species.

3. Ultrafast dissociation as a tool for novel physics

Coincident measurements of electrons and ions following the interaction of ionizing radiation with dilute matter is a powerful technique for tracking the flow of the energy deposited in the system by the absorption of a photon. Perhaps the most familiar electron-ion coincidence experiments at synchrotron light sources are the Cold Target Recoil Ion Momentum Spectroscopy, COLTRIMS, or "reaction microscope" instruments [21] which use opposing time-of-flight electron and ion spectrometers equipped with large area time and position sensitive charged particle detectors to collect ions and low energy electrons over the full 4π emission sphere. These exquisite instruments are used to determine the momenta of all of the charged particles emerging from the interaction of short wavelength light with atoms, molecules and clusters. Intricate details about ionization and molecular dynamics have been obtained with these instruments using 3rd generation synchrotron light sources, charged particle beams and ultrafast lasers. These instruments are not well suited to measuring ions in coincidence with electrons with high kinetic energy, however. Our group has therefore developed an alternative electron-ion coincidence spectrometer specifically to detect ions in coincidence with high energy electrons and it has been given the name EPICEA[1] [22].

High kinetic energy electrons in the EPICEA instrument are energy dispersed using a double toroidal electron energy analyzer fitted with a set of conical lenses to obtain a spectral resolution of 0.5–0.8% of the analyzer pass energy while collecting a solid angle of 4.2% of the full 4π sphere of emission for kinetic energies up to 500 eV [23]. Opposite to the electron energy analyzer

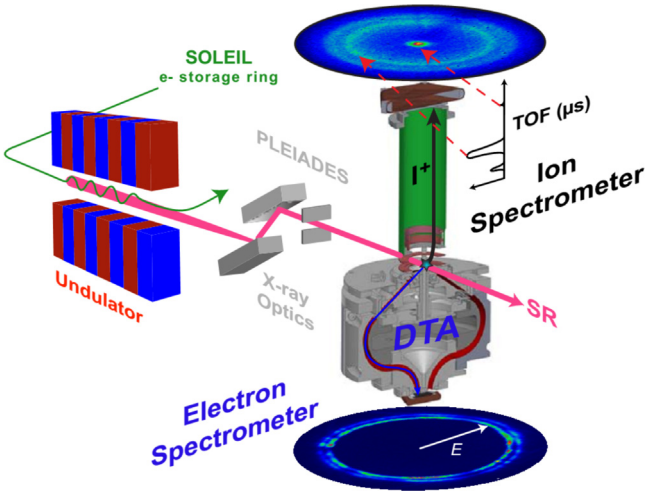

Fig. 4. Schematic/engineering drawing of the EPICEA high kinetic energy electron – ion momentum coincidence imaging instrument on the PLEIADES beamline at the SOLEIL synchrotron. Electrons are energy analyzed by the double toroidal analyzer (DTA) and the energy and angle of ejection of electrons measured with a position sensitive detector. Ions are extracted into the ion time-of-flight (TOF) spectrometer with 3D focusing optics. The flight times and positions of each ion are measured using a time and position sensitive detector allowing the momentum of each ion to be determined.
Reproduced from Ref. [24].

a 3D focusing ion time-of-flight spectrometer is used to detect the resulting ions as shown in the diagram of the system in Fig. 4. Delay line anode detectors capable of measuring the time and position of arrival of each particle are used for both electron and ion detection allowing the angular emission direction of the electron to be determined along with the momentum of the ion(s). Software has been developed to trigger extraction of ion(s) from the interaction region whenever an electron is detected, allowing the instrument to be used in the predominant multibunch operating mode at the synchrotron. Owing to the electron collection and detection efficiency of less than unity, false coincidences due to ions created without the associated electron detected will contribute random events to the measured signal. This background is corrected by a systematic measurement of the ion signal with randomly timed electrostatic extraction pulses that is subtracted from the coincident signal.

The EPICEA instrument was recently used to illustrate the effects of knowledge about the path of a particle in a Young's double slit-type experiment [24], an analogy to the moving slit experiment that was proposed by Einstein and Bohr at the birth of quantum mechanics as a *gedanken* experiment to illustrate the complementarity principle [25,26]. In this recent experiment oxygen molecules were photoexcited to the dissociative O $1s \rightarrow \sigma^*$ resonance with monochromatic synchrotron radiation, initiating an ultrafast dissociation process. Auger electrons were measured in coincidence with the momentum resolved atomic oxygen ions using the EPICEA instrument. As in the ultrafast dissociation measurements discussed in the previous section, electrons from both molecular and atomic states of oxygen are observed however with the electron-ion coincidence measurement it is possible to correlate each electron with the mass and momentum of its coincident ion. Doppler splitting of the Auger lines from ultrafast dissociation of oxygen corresponds to a transfer of energy from the kinetic energy of the moving atom to the Auger electron [15], but equally the kinetic energy of the outgoing Auger electron imparts a recoil energy to the source, either molecular O_2 or atomic O depending on whether the molecule is intact or dissociated at the time at which the Auger decay occurs, resulting in a change in momentum that can be measured in the experiment.

[1] EPICEA is the French acronym for "Etude de PhotoIons en Coïncidence avec des Electrons Analysés".

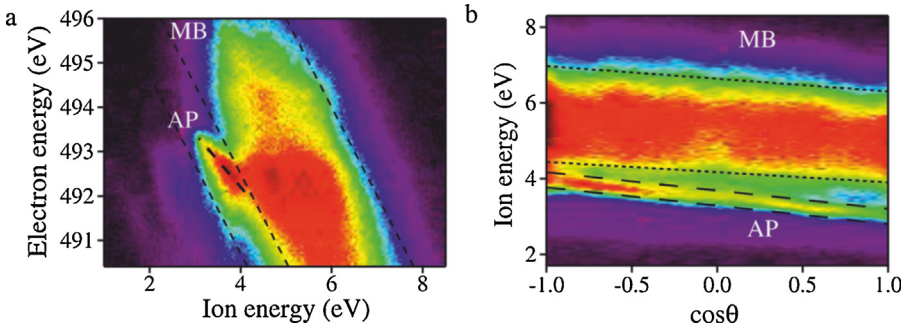

Fig. 5. Correlation maps of the (a) electron kinetic energy with the ion kinetic energy and (b) ion kinetic energy with the angle between the momenta of the electron and ion, θ following resonant excitation of the $O1s^{-1} \rightarrow 3\sigma_u$ state in O_2. MB refers to the molecular band and AP to the atomic peak as explained in the text. Modified from figure originally found in Ref. [24].

Passing over the fascinating quantum mechanical issue of the localization of the core hole in the homonuclear diatomic molecule O_2, emission of the energetic O-K Auger electron will impart significant recoil energy to the residual ion and if the ion is atomic rather than molecular the imparted momentum per atom will be doubled. This is clearly seen in Fig. 5(a) where the electron and ion energy correlation map for all coincidences is plotted. The slope of what is identified as the atomic peak (AP) is quite different from the overall slope of the much broader molecular band (MB). In the right hand panel of Fig. 5(b) the ion energy is shown as a function of the relative angle between the momenta of the ion and electron, θ, which can be determined from the coincident data by determining the angle of each electron and the momentum of each associated ion. The recoil of the ion is opposite to the Doppler shift for the electron, so an electron ejected opposite to the momentum of the ion ($\cos\theta = -1$) will increase the ion's kinetic energy, while an electron ejected along the momentum of the ion ($\cos\theta = 1$) will decrease its kinetic energy, trends that are apparent for both the molecular band and atomic peak in Fig. 5b. The lower mass of O versus O_2 results in an increased dependence of the kinetic energy of ions created by Auger decay from O^* versus those from $O_2{}^*$.

With these tools it is now possible to look at the electron energy as a function of its relative ejection angle which is shown in Fig. 6 for the molecular band in the top panels and the atomic peak in the bottom panels. For the electrons in the molecular band an interference pattern reminiscent of a Young's double slit pattern is observed. The interference is most obvious in the projection of a 1 eV wide band of electron kinetic energy into a line out in Fig. 6c were the data is compared with theoretical results that are shown in the correlation map in Fig. 6b and described in greater detail in Ref. [24]. Electrons from Auger decay in atomic oxygen show no interference, only a uniform intensity that disperses with relative angle due to the Doppler effect as shown in the lower panels for the experimental (Fig. 6d), theoretical (Fig. 6e) and integrated signal projected into a one dimensional curve in Fig. 6f.

The data was interpreted in the framework of the moving double slit *gedanken* experiment proposed by Einstein and Bohr [25,26]. When the Auger decay occurs in a molecular state of oxygen where the O 1s electrons are delocalized into gerade and ungerade molecular orbitals covering both atoms, the origin of each electron within the molecule cannot be uniquely assigned to one atom or the other and the interference pattern is observed. When the electron originates from an individual oxygen atom following ultrafast dissociation of the molecule into two atoms, the recoil momentum imparted to the atomic ion upon the Auger decay identifies it as either an atom moving in the opposite or same direction as the electron. This momentum tagging serves to identify which atom the electron originated from (equivalent to which slit the light went through in a double slit experiment) and the interference pattern is no longer observed. Much greater detail, including the theoretical interpretation of the spectra, is included in the original paper and associated supporting materials [24].

4. Mapping cationic and core-excited molecular potentials through nuclear dynamics

Molecular dynamics induced by excitation of core electrons can also be used to image molecular potentials by resonant photoemission. If, rather than causing a molecular dissociation, excitation of a core electron to an unoccupied molecular orbital below the continuum initiates a change in the geometry of the molecule, the core-hole lifetime clock can be used to probe the evolution of that geometry through its electronic decay. Bound and dissociative final cationic states are useful in different ways in this process to image the molecular potentials of the final states and the intermediate excited states respectively as outlined below.

Core level excited *initiated* – core hole lifetime *probed* dynamics have recently been used to examine both the nature of the core excited state and the extended form of the potential energy surface of the final inner valence cationic states by resonant photoemission. Inner valence ionized states of molecules, even when bound, often have significantly different equilibrium bond lengths than the ground electronic state of the molecule, so much different in fact that there is no overlap with the range of bond lengths populated in the ground vibrational state of the ground electronic state. According to the Franck Condon principle, therefore, these states cannot be accessible directly from the ground state by one photon since the overlap integrals for the nuclear wavefunctions are zero. Direct dipole transitions to some inner valence cationic states can also be forbidden due to symmetry selection rules and therefore cannot be accessed by single photon ionization from the ground state. Nevertheless these states can be important in reactivity, highly excited plasmas and multiphoton excitation pathways so information about their identification and the shape of their potentials is required.

Inner valence states of N_2 were studied recently using resonant photoexcitation of the bound $N1s^{-1}\sigma^*$ state of molecular N_2 as an intermediate step to drive nuclear dynamics, in this case elongation of the N-N bond, prior to resonant photoemission. Previously undetected $1^2\phi_g$ and $1^2\Delta_u$ cationic states were observed by this method and it was used to accurately map the potential energy curves of the $1^2\Pi_g$ and $1^2\phi_g$ cationic states both of which have considerably longer equilibrium bond lengths than the ground state [27]. To access the elongated bond lengths, narrow bandwidth X-ray radiation was used to selectively excite N 1s electrons of the molecule to various vibrational levels, in this case up to v = 6, of the intermediate $N1s^{-1}\sigma^*$ core hole state as shown in Fig. 7a and 7b. The vibrationally resolved photoabsorption profile of the $N1s^{-1}\sigma^*$ state is shown on the right of the figure in panel b and aligned with

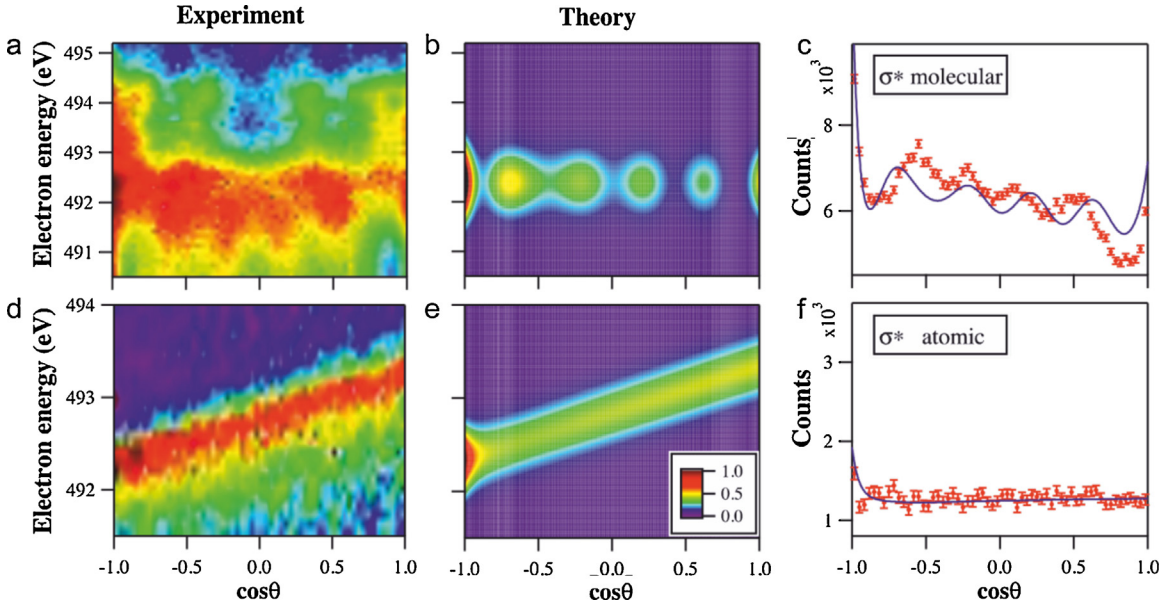

Fig. 6. Comparison between experimental and theoretical Auger electron kinetic energies and their respective projections into one dimension for (a–c) molecular decay of the $O1s^{-1} \rightarrow 3\sigma_u$ state in O_2 and (d–f) atomic decay of the $O1s^{-1} \rightarrow 3\sigma_u$ state in O_2 following ultrafast dissociation. The results are discussed in the text.
Modified from a figure originally reported in Ref. [24].

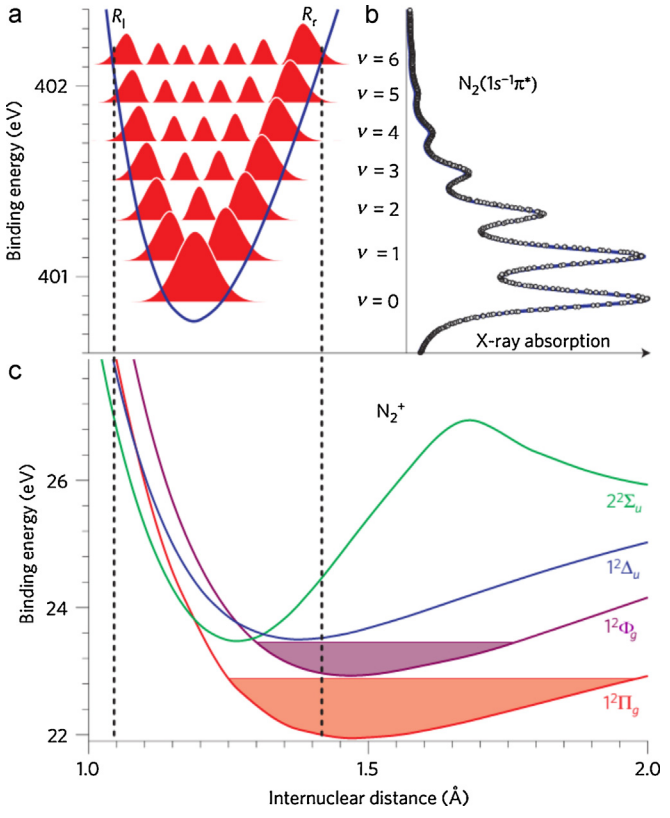

Fig. 7. (a) The potential energy curve and nodal structure of the vibrational wavefunctions for the first seven vibrational levels of the core excited $N1s^{-1}\pi^*$ state of N_2. (b) The X-ray absorption spectrum corresponding to excitation of a N1s electron into the vibration levels of the core excited $N1s^{-1}\pi^*$ state of N_2. (c) Potential energy curves for some of the inner valence states of N_2^+ on the same internuclear distance axis as the core excited potential energy curve in panel a. The dashed lines indicate left – the equilibrium nuclear bond length for N_2 in the ground state and right – the position of the lobe on the outer turning point of the $v = 6$ vibrational level of the core excited state.
Modified from Ref. [27].

the vibrational wavefunction amplitudes on the potential energy curve of this state on the left in panel a of Fig. 7.

High resolution resonant photoemission then imaged the overlap of the excited state populations with the cationic inner valence states. In the case of the $1^2\Pi_g$ and $1^2\phi_g$ cationic states high vibrational levels of the core excited state were essential to access the elongated bond lengths of these states at the outer turning point of the vibrational wavefunction of the $v = 6$ vibrational level, indicated as R_r in Fig. 7a. Excitation from the ground state, with an equilibrium bond length of 1.04 Å populates the inner turning point of this level, R_I, as indicated by the dashed line on the left hand side of Fig. 7a. During the lifetime of the core hole, 5.7 ± 0.2fs, the electronic wavepacket of the vibrationally excited $N1s^{-1}\sigma^*$ state has time to evolve to cover the entire vibrational envelope before the resonant photoemission process projects it down onto the lower inner valence cationic state as illustrated by the dashed line on the right hand side of Fig. 7a. At his elongated bond length of over 1.4 Å there is sufficient overlap with the vibrational levels of the $1^2\Pi_g$ and $1^2\phi_g$ cationic states, as shown by the dashed line extending down to the potential energy curves of these states in Fig. 7c, to allow observation of the vibrational progressions. High spectral resolution resonant photoemission spectra were obtained and were essential for mapping the potential energy curves of these final states. Vibrational progressions resolved in the resonant photoemission spectra were fit to obtain the potential energy curves and spectroscopic parameters. Good agreement was found for the spectroscopic parameters for the $1^2\Pi_g$ state which has been rovibrationally resolved previously and fit by standard techniques. The $1^2\phi_g$ state was observed for the first time, so its parameters could not be compared.

A more detailed investigation of the inner valence ionic states of N_2 with binding energies between 22 and 34 eV was also reported [28] using high resolution resonant photoemission spectroscopy. Nine excitation energies around the $N1s^{-1} \rightarrow \pi^*$ resonance were used and the results compared with configuration interaction ab initio calculations to aid in the interpretation of the data. Twelve final electronic states were observed and characterized. As in the previous study, access to elongated N—N bond lengths through

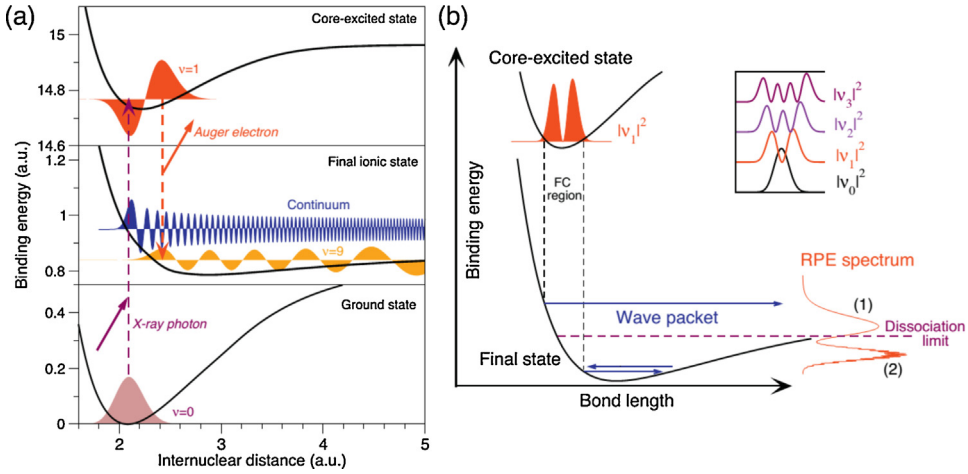

Fig. 8. Schematic representation of the wavefunction mapping technique to map the nodal structure of the wavefunctions of the vibrational levels of a core excited state. (a) Shows the potential energy curves and wavefunction nodal structure for the ground state (lower panel), core-excited state (upper panel) and final ionic state (middle panel) that is reached indirectly from the ground state through the core-excited state. (b) Illustrates the projection of the two lobe nodal structure of the intermediate core-excited state onto the potential energy surface of the final ionic state and the resulting resonant photoelectron spectrum (RPE). In this generic example the left-most lobe of the core-excited state wavefunction projects below the dissociation limit of the final state and the right-most lobe above the dissociation limit but both are still apparent in the RPE spectrum. The nodal structures of the first four vibrational core-excited states are shown in the upper right hand side of the panel. A detailed discussion is given in the text.

From Ref. [29].

higher vibrational levels of the intermediate state was essential to characterizing the final states.

Vibrational wave function mapping of the intermediate core excited state was also reported for this data and compared with the results from other molecules in a review of the technique [29]. Briefly, wavefunction mapping uses the reflection principle [30] to project the electron population density of the vibrational wavefunctions of the core excited state onto dissociative surfaces of the final states. In cases where part of the wavefunction overlaps with bound states, the distribution of intensity can still be used to map the wavefunction as explained in Refs. [28,29] and illustrated in Fig. 8. As shown in panel a of this figure (top, left), the $v=1$ vibrational level of the core excited states (with two lobes) is populated by excitation with an X-ray photon. The wavefunction spreads out over the allowed geometry for this state and upon deexcitation to the final ionic state the lobe at the inner turning point of the core excited potential overlaps with the continuum while the lobe at the outer turning point overlaps with the $v=9$ vibrational level of the bound state. The right hand panel of Fig. 8, panel b, shows the deexcitation step in greater detail, but with the same ideas. The left hand lobe of the wavefunction overlaps with dissociative part of the potential energy curve of the final state and is projected as a broad featureless continuum in the resonant photoemission spectrum (1). The right hand lobe of the wavefunction overlaps with bound portion of the final state potential and populates its manifold of vibrational states and appears as a set of vibrationally resolved peaks in the resonant photoemission spectrum (2).

In the long range resonant photoemission spectra in the $N1s^{-1} \rightarrow \pi^*$ excited N_2 some features of the nodal structure of the vibrational wavefunctions of the core excited states were identified. But overlapping contributions to the overall vibronic envelope hampered unambiguous assignments to specific lobes in the core excited state of this molecule.

Vibrationally and angularly resolved resonant photoemission measurements were also reported recently for O_2 and used to identify interferences between the direct and $O1s^{-1} \rightarrow \sigma^*$ resonant paths to the same $X\ ^2\Pi_g$ cationic final states [31]. The interferences give rise to variations in the anisotropy parameter, β, when both direct and resonant paths to the final state are accessible. Only vibrational levels up to $v=6$ are populated for the $X\ ^2\Pi_g$ state by direct photoionization, hence these states exhibit the anomalous asymmetry parameters, while resonant excitation populates this state to much higher vibrational levels. Higher vibrational levels do not interfere with direct channels as they are not accessible by direct photoionization from the ground state and exhibit a constant value for the asymmetry parameter.

5. Conclusions

Synchrotron radiation, and in particular high spectral resolution synchrotron radiation from 3rd generation light sources is a powerful tool for studying molecular dynamics in small molecules. Promotion of core electron to an unoccupied molecular orbital below the ionization potential initiates a dynamic response from the molecule; either a dissociation when an antibonding orbital is populated, or a change in the molecular geometry if a non-bonding or a bonding orbital is accessed and functions as a pump. The highly energetic core hole configuration of the molecule decays via an Auger decay with a characteristic lifetime which can be used as a probe to examine the dynamic response of the molecule to the pump. Molecular dissociation following excitation of an O 1s core electron to and antibonding orbital in O_2 was used to investigate an analog to the moving slit Young's double slit experiment proposed by Einstein and Bohr. Interferences in the emission of electrons observed when they are ejected from the molecule disappear when Doppler recoil momentum tagging is used to determine the atomic origin of the electron, the equivalent of knowing which slit light goes through in a conventional double slit experiment. High resolution resonant photoemission via high vibrational levels of core excited states were shown to be powerful tools for mapping and understanding the complex inner valence cationic states of molecules, states that are sometimes not otherwise accessible. Elongation of the molecular bond in the intermediate core excited state was used to access these states allowing them to be identified and characterized. In all cases high level quantum mechanical calculations were required for the interpretation of the data. These examples, all depending on access to intense high-resolution synchrotron radiation and state-of-the art electron energy analyzers and coincidence apparatus, show that high quality synchrotron X-ray sources are essential tools in the study of molecular dynamics.

Acknowledgements

The contributions of our colleagues on the PLEIADES beamline at Synchrotron SOLEIL Christophe Nicolas, Minna Patanen and Emmanuel Robert and our former colleague Xiao-Jing Liu are gratefully acknowledged, as is the great inspiration and guidance for theoretical interpretation from Faris Gel'mukhanov and his coworkers. CM acknowledges funding from "Laboratoire d'Excellence Physics Atoms Light Matter" (LabEx PALM) overseen by the French National Research Agency (ANR) as part of the "Investissements d'Avenir" program (reference: ANR-10-LABX-0039) and the European COST action CM1204 – XUV/X-ray light and fast ions for ultrafast chemistry (XLIC).

References

[1] E. Allaria, L. Badano, S. Bassanese, F. Capotondi, D. Castronovo, P. Cinquegrana, M.B. Danailov, G. D'Auria, A. Demidovich, R. De Monte, G. De Ninno, S. Di Mitri, B. Diviacco, W.M. Fawley, M. Ferianis, E. Ferrari, G. Gaio, D. Gauthier, L. Giannessi, F. Iazzourene, G. Kurdi, N. Mahne, I. Nikolov, F. Parmigiani, G. Penco, L. Raimondi, P. Rebernik, F. Rossi, E. Roussel, C. Scafuri, C. Serpico, P. Sigalotti, C. Spezzani, M. Svandrlik, C. Svetina, M. Trovó, M. Veronese, D. Zangrando, M. Zangrando, J. Synchrotron Radiat. 22 (2015) 485.
[2] W.E. White, A. Robert, M. Dunne, J. Synchrotron Radiat. 22 (2015) 472.
[3] M. Yabashi, H. Tanaka, T. Ishikawa, J. Synchrotron Radiat. 22 (2015) 477.
[4] B. Erk, R. Boll, S. Trippel, D. Anielski, L. Foucar, B. Rudek, S.W. Epp, R. Coffee, S. Carron, S. Schorb, K.R. Ferguson, M. Swiggers, J.D. Bozek, M. Simon, T. Marchenko, J. Kupper, I. Schlichting, J. Ullrich, C. Bostedt, D. Rolles, A. Rudenko, Science 345 (2014) 288.
[5] K. Schnorr, A. Senftleben, M. Kurka, A. Rudenko, G. Schmid, T. Pfeifer, K. Meyer, M. Kubel, M.F. Kling, Y.H. Jiang, R. Treusch, S. Dusterer, B. Siemer, M. Wostmann, H. Zacharias, R. Mitzner, T.J.M. Zouros, J. Ullrich, C.D. Schroter, R. Moshammer, Phys. Rev. Lett. 113 (2014) 073001.
[6] R. Feifel, M.N. Piancastelli, J. Electron Spectrosc. Relat. Phenom. 183 (2011) 10.
[7] P. Morin, C. Miron, J. Electron Spectrosc. Relat. Phenom. 185 (2012) 259.
[8] K. Ueda, J. Phys. Soc. Jpn. 75 (2006) 032001.
[9] C. Miron, C., Nicolas, M., Patanen, J.D. Bozek, http://www.synchrotron-soleil.fr/Recherche/LignesLumiere/PLEIADES.
[10] P. Morin, I. Nenner, Phys. Rev. Lett. 56 (1986) 1913.
[11] H. Aksela, S. Aksela, H. Pulkkinen, G.M. Bancroft, K.H. Tan, Phys. Rev. A 33 (1986) 3876.
[12] P. Morin, I. Nenner, Phys. Scr. T17 (1987) 171.
[13] X.M. Feng, A.A. Wills, E. Sokell, M. Wiedenhoeft, N. Berrah, Phys. Rev. A 73 (2006) 012716.
[14] P. Lablanquie, H. Iwayama, F. Penent, K. Soejima, E. Shigemasa, J. Electron Spectrosc. Relat. Phenom. 195 (2014) 96.
[15] O. Björneholm, M. Bässler, A. Ausmees, I. Hjelte, R. Feifel, H. Wang, C. Miron, M.N. Piancastelli, S. Svensson, S.L. Sorensen, F. Gel'mukhanov, H. Ågren, Phys. Rev. Lett. 84 (2000) 2826.
[16] R. Feifel, Y. Velkov, V. Carravetta, C. Angeli, R. Cimiraglia, P. Salek, F. Gel'mukhanov, S.L. Sorensen, M.N. Piancastelli, A. De Fanis, K. Okada, M. Kitajima, T. Tanaka, H. Tanaka, K. Ueda, J. Chem. Phys. 128 (2008) 064304.
[17] M. Simon, R. Püttner, T. Marchenko, R. Guillemin, R.K. Kushawaha, L. Journel, G. Goldsztejn, M.N. Piancastelli, J.M. Ablett, J.-P. Rueff, D. Céolin, Nat. Commun. 5 (2014) 4069.
[18] C. Miron, Q. Miao, C. Nicolas, J.D. Bozek, W. Andrałojć, M. Patanen, G. Simões, O. Travnikova, H. Ågren, F. Gel'mukhanov, Nat. Commun. 5 (2014) 3816.
[19] D. Ceolin, O. Travnikova, Z. Bao, A. Kivimaki, S. Carniato, M.N. Piancastelli, J. Electron Spectrosc. Relat. Phenom. 184 (2011) 24.
[20] O. Travnikova, V. Kimberg, R. Flammini, X.J. Liu, M. Patanen, C. Nicolas, S. Svensson, C. Miron, J. Phys. Chem. Lett. 4 (2013) 2361.
[21] R. Dorner, V. Mergel, O. Jagutzki, L. Spielberger, J. Ullrich, R. Moshammer, H. Schmidt-Bocking, Phys. Rep. – Rev. Sect. Phys. Lett. 330 (2000) 95.
[22] X.J. Liu, C. Nicolas, E. Robert, C. Miron, IOP, XXVIII International Conference on Photonic, Electronic and Atomic Collisions (ICPEAC), vol. 488, 2014, p. 142005.
[23] X.J. Liu, C. Nicolas, C. Miron, Rev. Sci. Instrum. 84 (2013) 033105.
[24] X.-J. Liu, Q. Miao, F. Gel'mukhanov, M. Patanen, O. Travnikova, C. Nicolas, H. Ågren, K. Ueda, C. Miron, Nat. Photon. 9 (2015) 120.
[25] N. Bohr, Quantum Theory and Measurement, Princeton University Press, 1983.
[26] W.K. Wootters, W.H. Zurek, Phys. Rev. D 19 (1979) 473.
[27] C. Miron, C. Nicolas, O. Travnikova, P. Morin, Y.P. Sun, F. Gel'mukhanov, N. Kosugi, V. Kimberg, Nat. Phys. 8 (2012) 135.
[28] V. Kimberg, A. Lindblad, J. Soderstrom, O. Travnikova, C. Nicolas, Y.P. Sun, F. Gel'mukhanov, N. Kosugi, C. Miron, Phys. Rev. X 3 (2013) 011017.
[29] V. Kimberg, C. Miron, J. Electron Spectrosc. Relat. Phenom. 195 (2014) 301.
[30] G. Herzberg, Spectra of Diatomic Molecules, van Nostrand Reinhold, New York, 1950.
[31] A. Lindblad, V. Kimberg, J. Soderstrom, C. Nicolas, O. Travnikova, N. Kosugi, F. Gel'mukhanov, C. Miron, N. J. Phys. 14 (2012) 113018.